

Applied stress controls the production of nano-twins in coarse-grained metals

Cite as: Appl. Phys. Lett. **101**, 231903 (2012); <https://doi.org/10.1063/1.4769216>

Submitted: 14 August 2012 • Accepted: 14 November 2012 • Published Online: 04 December 2012

Y. Cao, Y. B. Wang, X. Z. Liao, et al.



View Online



Export Citation



CrossMark

ARTICLES YOU MAY BE INTERESTED IN

[Nucleation of deformation twins in nanocrystalline face-centered-cubic metals processed by severe plastic deformation](#)

Journal of Applied Physics **98**, 034319 (2005); <https://doi.org/10.1063/1.2006974>

[Nucleation and growth of deformation twins in nanocrystalline aluminum](#)

Applied Physics Letters **85**, 5049 (2004); <https://doi.org/10.1063/1.1823042>

[Deformation twinning in nanocrystalline copper at room temperature and low strain rate](#)

Applied Physics Letters **84**, 592 (2004); <https://doi.org/10.1063/1.1644051>



Trailblazers. ^{New}

Meet the Lock-in Amplifiers that measure microwaves.

Zurich Instruments [Find out more](#)

Applied stress controls the production of nano-twins in coarse-grained metals

Y. Cao,¹ Y. B. Wang,¹ X. Z. Liao,^{1,a)} M. Kawasaki,^{2,3} S. P. Ringer,^{1,4} T. G. Langdon,^{2,5} and Y. T. Zhu⁶

¹*School of Aerospace, Mechanical and Mechatronic Engineering, The University of Sydney, Sydney, NSW 2006, Australia*

²*Departments of Aerospace & Mechanical Engineering and Materials Science, University of Southern California, Los Angeles, California 90089-1453, USA*

³*Division of Materials Science and Engineering, Hanyang University, 17 Haengdang-dong, Seongdong-gu, Seoul 133-791, South Korea*

⁴*Australian Centre for Microscopy & Microanalysis, The University of Sydney, Sydney, NSW 2006, Australia*

⁵*Materials Research Group, Faculty of Engineering and the Environment, University of Southampton, Southampton SO17 1BJ, United Kingdom*

⁶*Department of Materials Science and Engineering, North Carolina State University, Raleigh, North Carolina 27695, USA*

(Received 14 August 2012; accepted 14 November 2012; published online 4 December 2012)

We present evidence that the level of the applied stress plays a critical role in deformation twinning in face-centred cubic alloys. While conventional cold rolling of a face-centred cubic structure produces a microstructure with a high-density of extended dislocations, increasing the applied stress using high-pressure torsion gives a nano-twinned coarse-grained structure. This suggests the existence of a critical stress for deformation twinning which thereby delineates an approach for the production of nano-twinned microstructures in coarse-grained materials with superior mechanical properties. © 2012 American Institute of Physics. [<http://dx.doi.org/10.1063/1.4769216>]

Nano-twins in metallic materials have been reported to significantly improve strength and ductility¹⁻⁵ while retaining good corrosion resistance^{6,7} and electrical conductivity.¹ The simultaneous improvement of strength and ductility is possible because high densities of twin boundaries serve to block and trap gliding dislocations.⁸ The corrosion resistance and the electrical conductivity are preserved by the low energy nature of the twin boundaries.^{1,6,7} Nano-twins can be produced via many methods, including materials synthesis using electro-deposition^{1,9} and materials processing using plastic deformation.¹⁰⁻¹² Electro-deposition is a bottom-up slow synthesis method that produces grain sizes usually limited to the sub-micrometer range. While a slow synthesis process is a serious problem for large-scale production of materials, small grain sizes introduce an excess of high-energy grain boundaries that lower the electrical conductivity of materials.^{1,6,7} The lack of the flexibility of grain size control also limits the number of options available to manipulate the mechanical properties of materials.¹³ By contrast, producing nano-twins via plastic deformation has proved to be a rapid, effective approach for materials with low stacking fault energies, and can be used to produce nano-twinned materials with quite large grain sizes ($>1 \mu\text{m}$).^{10,12}

Deformation twinning can be affected by many factors,¹⁴⁻¹⁷ including stacking fault energy,^{18,19} grain size,²⁰⁻²³ grain orientation,^{24,25} strain,¹² strain rate,^{19,26} and temperature.^{10,26} Stacking fault energy is an intrinsic material property that is fixed for a specific composition. Grain size and grain orientation are microstructural characteristics that can be modified but at the cost of time and energy. Increasing

strain and strain rate, and/or reducing processing temperature, are reported to promote deformation twinning.^{15,17} The intrinsic reason determining the twinning behaviour is not clear. Nevertheless, the common factor of these deformation conditions is their relatively high flow stress. This raises a question: is the applied stress the determining factor for the activation of deformation twinning? In this report, we demonstrate that increasing the applied stress to levels above the critical stress for deformation twinning leads to significant changes in the deformation mode and produces very high densities of deformation twins in a face-centred cubic (FCC) metallic structure.

Two different deformation methods, cold rolling and high-pressure torsion (HPT), were used to produce different levels of applied stresses during the deformation of a commercial DP3W duplex stainless steel. This steel has approximately equal volume fractions of FCC austenite and body-centred cubic (BCC) ferrite phases. While the austenite was used to investigate the effect of pressure on the deformation behaviour in FCC structures, the ferrite provided a comparison of the imposed plastic strain in samples processed by different methods since changing the applied pressure does not change the deformation mode in the BCC structures. Detailed information on the duplex stainless steel was reported earlier.^{27,28} As-received steel plates with an original thickness of 3 mm were cold rolled many times to reach a final thickness of 110 μm , which gives an equivalent strain $\varepsilon = \sim 3$. For HPT deformation, two disk samples with a diameter of 1 cm and a thickness of 0.8 mm were deformed under quasi-constrained conditions^{29,30} for 1 revolution under an applied pressure of 6 GPa at 1 rpm rotation speed.

Specimens for transmission electron microscopy (TEM) investigation were prepared using mechanical grinding

^{a)} Author to whom correspondence should be addressed. Electronic mail: xiaozhou.liao@sydney.edu.au. Tel.: +61 2 93512348.

followed by electro-polishing at room temperature using standard techniques. The TEM specimens were cut from HPT disks in regions close to the centre of the disk where the equivalent strain was less than 2. TEM characterisation was performed using a Philips CM12 for diffraction contrast imaging and a JEOL 3000F for atomic resolution imaging. An IBIS nanoindentation system was used to obtain the hardness data from the as-received, cold rolled, and HPT samples. Details on the sample preparation for indentation testing are described elsewhere.²⁸ The indentation was performed using a Berkovich indenter tip under the force control mode with a maximum load of 28 mN. The hardness of the as-received and cold-rolled samples was obtained by averaging more than 25 indents with spacing of 100 μm on each sample. The error bar for each average hardness value was obtained from the highest to the lowest value recorded. Nanoindentation on the HPT disks was conducted along two mutually perpendicular diameters by collecting 200 indent datum points at intervals of 40 μm along each diameter.

The average grain sizes of both the FCC and BCC phases in the as-received material were $\sim 8 \mu\text{m}$. Grains in the as-received material exhibited smooth, sharp grain boundaries. The dislocation density in the as-received material was very low and, predictably, cold rolling dramatically changed the microstructure. Figure 1 shows the typical microstructure of the FCC grains in a cold rolled sample observed along a direction close to a $\langle 110 \rangle_{\gamma}$. A high density of low-angle grain boundaries and dislocation walls was formed to divide the originally large FCC grains into sub-grains with diameters in the range of 200–1000 nm (see Fig. 1(a)). The area marked with a white rectangle in Fig. 1(a) is enlarged in Fig. 1(b), revealing the detailed microstructure of a dislocation wall. An extremely high density of dislocations was observed around these dislocation wall areas. Because the FCC austenite has a very low stacking fault energy,^{2,31} these dislocations appear as straight parallel lines. They are actually extended dislocations with each having two partial dislocations at the two ends of a line and a stacking fault lying in-between on a $\{111\}_{\gamma}$ plane.³² The interval between the two partial dislocations was up to 100 nm. The inset in Fig. 1(b) is an electron diffraction pattern recorded along a $\langle 110 \rangle_{\gamma}$ zone axis of the area in Fig. 1(b). Diffraction spots are slightly extended forming diffraction arcs, indicating a small misorientation in the area caused by the dislocation walls. Figure 1(c) shows an atomic resolution image of a few extended dislocations marked by white arrows, confirming that most of the parallel lines seen in Fig. 1(b) are indeed extended dislocations with a stacking fault bordered by a pair of partial dislocations. Extensive investigations of these sorts of atomic resolution images indicated that, while most of the parallel lines in the cold-rolled material were extended dislocations, some were very thin nano-twins with thicknesses of a few atomic layers and widths of not more than 100 nm. Such nano-twins could be formed via the dynamic overlap of two or more extended partial dislocations with stacking faults on adjacent slip planes.^{21,33} However, no twin extending through a whole grain was observed. These results indicate that the plastic deformation in the FCC austenite phase under a conventional cold rolling process with relatively small applied pressure was dominated by dislocation slip. It is also worth noting

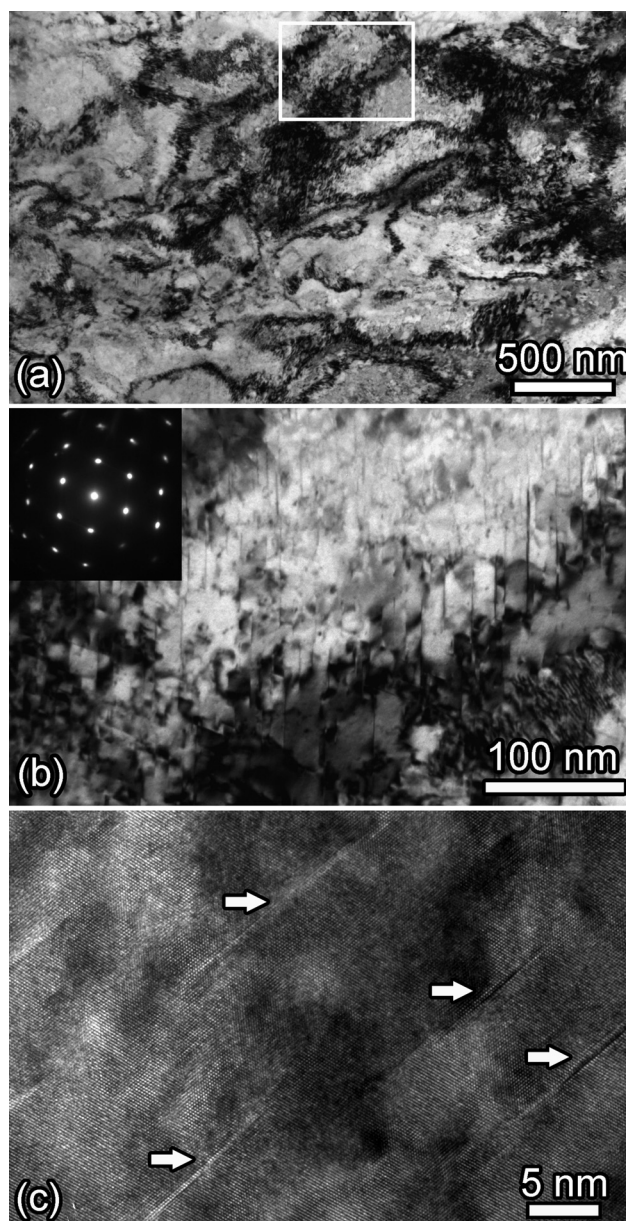


FIG. 1. (a) A typical TEM image of austenite grains in a cold rolled sample with strain of ~ 3 ; (b) a magnified image of the area marked with a white rectangle in (a); and (c) an atomic resolution image showing stacking faults, which are marked by white arrows in an austenite grain.

that the BCC ferrite grains in the cold-rolled samples were refined to the sub-micrometer size range. This grain refinement process was dominated by dislocation motion, as deformation twinning was rarely observed.

By contrast, a very different microstructure was observed in the FCC austenite in the HPT disks. Figure 2(a) shows a typical TEM image of FCC grains at an area close to the centre of an HPT disk. Because only small strains were applied to these regions, the FCC phase retains the same grain sizes and morphology as the as-received state. However, all FCC grains possessed a very high density of deformation twins that extended throughout the grain. On the other hand, the neighbouring BCC ferrite phase retained sharp, smooth grain boundaries (shown in Fig. 2(b) and marked with white arrows), although a very high density of tangled dislocations (marked by black arrows in Fig. 2(b))

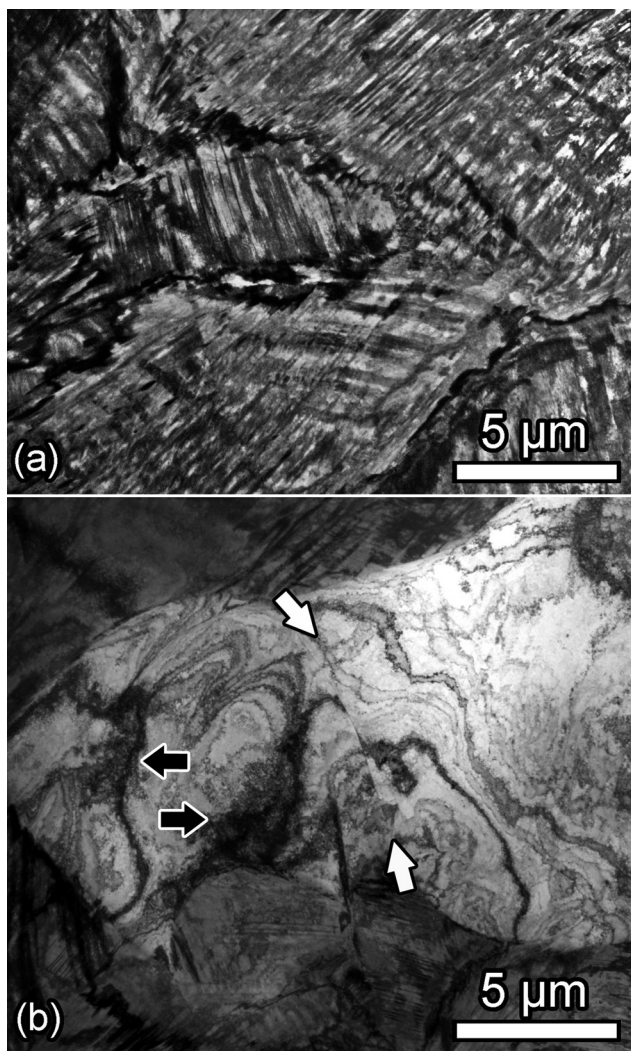


FIG. 2. (a) A typical TEM image of austenite grains in a low strained area close to the centre of an HPT disk; (b) a typical TEM image of ferrite and austenite grains in the same area. White arrows mark a sharp and straight grain boundary between two ferrite grains. Black arrows indicate areas with dislocation tangling.

was also observed in the BCC phase. The sharp, smooth grain boundaries in the HPT disks indicate that the shear strain applied to these areas was very low and is much lower than in the cold-rolled sample where the BCC grains were refined down to the sub-micrometer size range.

While the grain sizes of the observed HPT sample area remain the same as for the as-received material, the twins formed inside the grains exhibit a twin boundary spacing (TBS) of less than 30 nm. Figure 3(a) presents a typical image of nano-sized deformation twins formed inside a large FCC grain. Figure 3(b) provides statistical data on the distribution of the TBS measured from more than 10 individual grains. Most of the nano-twins have TBS of ~ 5 nm while TBS of larger than 30 nm was not seen. A comparison of the TBS of HPT disks processed under 2 GPa (data not presented here) and 6 GPa shows that the applied stress does not have a significant effect on the TBS provided the stress is sufficiently high to trigger deformation twinning. The mechanism behind this phenomenon has not been understood. It is also not clear if the phenomenon is common in other FCC materials. Further investigation is needed to clarify these issues.

Figure 3(c) is an atomic resolution image of these nano-twins. Because the nano-twins and the matrix are of similar widths, they are not distinguishable indicating that the nano-twin density achieved an equilibrium state under the current deformation.¹² Figure 3(d) shows a one-dimensional Fourier-filtered image of Fig. 3(c). Black arrows in Fig. 3(d) indicate the twin boundary positions observed in Fig. 3(c), and the two black “T” marks represent two full dislocations. The two dislocations glided along a $\{111\}_\gamma$ plane that forms an angle of $70^\circ 32'$ with the nano-twin planes. The fact that the dislocations are located at twin boundaries indicates that the motion of the dislocations was stopped by the twin boundaries. We suggest that the high pressure applied to the material and the interaction between the dislocations and the twin boundaries are responsible for the combination of partial dislocations into full dislocations.^{34,35}

Statistical analyses of numerous atomic resolution images (Fig. 3) indicated that the average dislocation density in these nano-twinned grains was $\sim 4.6 \times 10^{16} \text{ m}^{-2}$ which is a typical dislocation density in heavily deformed metallic materials.^{36,37} This indicates that both deformation twinning and dislocation motion play a significant role in the deformation of the FCC phase during the HPT deformation.

TEM investigation of HPT samples with strain values close to or slightly higher than 3 (i.e., further away from the disk centre) indicates that the grain size and microstructure of the BCC phase were very similar to that observed in the cold-rolled sample, and the FCC phase was also full of nano-twins with TBS similar to that reported in Fig. 3. However, the average dislocation density was further increased to $\sim 9.2 \times 10^{16} \text{ m}^{-2}$ with more dislocations trapped at twin boundaries, indicating that dislocation slip dominates further plastic deformation after the twin thickness reaches the saturation level.

Although cold rolling and HPT produce two distinct microstructures in the FCC phase, the two processing methods offer similar hardness when the shear strains applied in the two processes are similar. Figure 4 presents the hardness of the as-received, cold-rolled, and HPT samples as a function of equivalent strain. The hardness of the as-received material was ~ 3.6 GPa. After cold rolling to a strain of ~ 3 , the hardness reached ~ 6.3 GPa which is about the same as the hardness of HPT samples at the same equivalent strain.

Dislocation slip and deformation twinning are two competitive deformation mechanisms. In coarse-grained materials, the critical stress for deformation twinning is normally higher than for dislocation slip. Therefore, dislocation slip usually occurs before twinning. With increased plastic strain, the dislocation density increases so that dislocation motion becomes more difficult (i.e., work hardening occurs) and so the flow stress increases. When the flow stress reaches the critical stress for twinning, the deformation twinning is activated. In the cold-rolled sample investigated here, dislocation slip dominates the deformation process leading to the formation of a high density of dislocations and dislocation cells. The latter would further evolve into low-angle grain boundaries and later to high-angle grain boundaries with additional plastic deformation. However, provided the flow stress is below the critical stress for twinning, the deformation process remains controlled by dislocation slip.

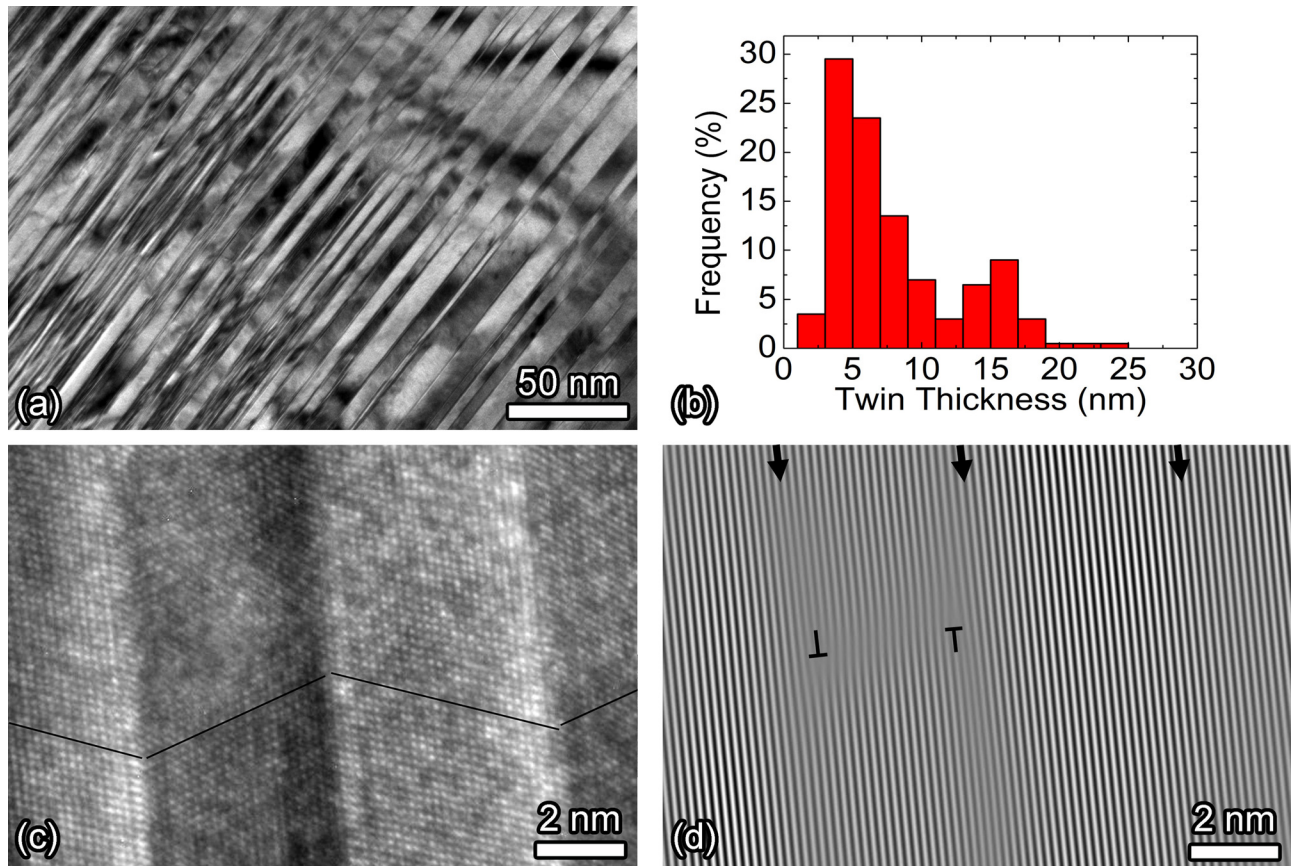


FIG. 3. (a) A high magnification TEM image showing nanotwins in an austenite grain; (b) the statistical distribution of TBS; (c) an atomic resolution image of nanotwins; (d) a one-dimensional Fourier-filtered image of (c). The black arrows in (d) indicate the positions of the twin boundaries seen in (c). Two black “T” mark the cores of two dislocations.

Processing by HPT is different from conventional plastic deformation techniques such as cold rolling where the flow stress can only be increased via work hardening. This is because HPT processing in the constrained or quasi-constrained mode can directly apply a pressure that is higher than the critical stresses for both dislocation slip and deformation twinning. Therefore, dislocation slip and deformation twinning occur simultaneously. This explains the co-existence of a high density of deformation twins and a high density of

dislocations in the FCC phase after small HPT strains. When the twin density becomes saturated, further deformation is dominated by dislocation slip that increases the dislocation density. Although the strain path of HPT is different from that of cold rolling,^{27,29,38} this does not affect our conclusion because it is the resolved shear stress applied to slip/twinning planes, not the strain path, that activates dislocation motion and deformation twinning. A similar conclusion was also reported recently that the formation mechanism of deformation twins does not depend on the deformation mode although the latter affects the morphology of deformation twins.³⁹ Similar phenomena of high stresses promoting deformation twinning were also reported in FCC materials processed by equal-channel angular pressing (ECAP) where high stresses are possible because of the high shear stresses introduced at the corners of the ECAP dies,^{37,40} In addition, the stacking fault energy also plays a critical role for the formation of a high density of deformation twins. Alloying is an effective way to reduce the stacking fault energy and therefore enable high densities of deformation twins.⁴¹

It is interesting to note that the two very different microstructures obtained by cold rolling and HPT provide similar hardness when the strain values for the two processing approaches are both ~ 3 . This is because both twin boundaries and dislocation walls are effective at blocking dislocation slip, resulting in hardening that follows the Hall-Petch relationship.^{42,43} Notably, the dislocation walls may transform into conventional grain boundaries at later stages of

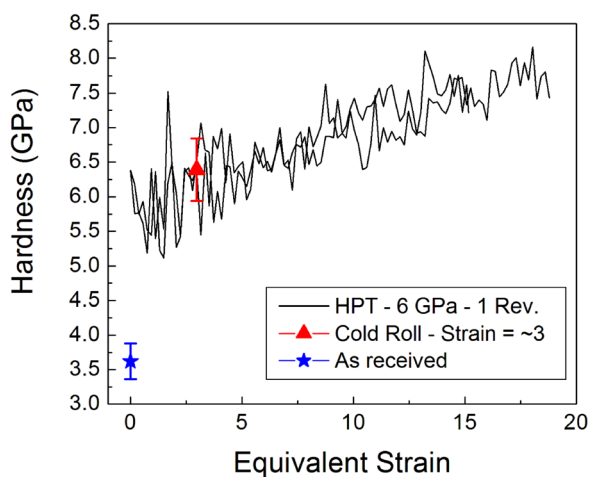


FIG. 4. The hardness of the as-received, cold-rolled, and HPT samples as a function of equivalent strain.

deformation. It follows that the nano-twinned coarse-grained structure exhibits better ductility⁸ and better electrical conductivity¹ and corrosion resistance.^{6,7} Further, it has been reported that the thermal stability of nano-twinned microstructures is superior to that of conventional grain boundaries.⁴⁴ Therefore, nano-twinned structures with superior mechanical properties may be useful for some high temperature engineering applications.

In summary, FCC materials with low stacking fault energies, such as austenitic steel, deform differently under low-pressure and high-pressure plastic deformation. For deformation under low-pressure, dislocation slip dominates the deformation. For deformation under high-pressure, two deformation mechanisms—twinning and dislocation slip—may be activated, simultaneously. These observations indicate that the applied stress controls the activation of deformation twinning. They also point to a strategy for producing nano-twinned coarse-grained microstructures in FCC materials to obtain superior mechanical and physical properties.

The authors acknowledge the scientific and technical input and support from the Australian Microscopy & Microanalysis Research Facility node at the University of Sydney. This project was supported by the Australian Research Council (Grant No. DP120100510 (Y.C., Y.B.W., and X.Z.L.)), the National Science Foundation of the United States (Grant No. DMR-1160966 (M.K. and T.G.L.)), and the National Science Foundation of the United States (Grant No. DMR-1104667 (Y.T.Z.)).

¹L. Lu, Y. Shen, X. Chen, L. Qian, and K. Lu, *Science* **304**, 422 (2004).

²X. Zhang, A. Misra, H. Wang, M. Nastasi, J. D. Embury, T. E. Mitchell, R. G. Hoagland, and J. P. Hirth, *Appl. Phys. Lett.* **84**, 1096 (2004).

³Y. H. Zhao, Y. T. Zhu, X. Z. Liao, Z. Horita, and T. G. Langdon, *Appl. Phys. Lett.* **89**, 121906 (2006).

⁴X. Zhang, H. Wang, X. H. Chen, L. Lu, K. Lu, R. G. Hoagland, and A. Misra, *Appl. Phys. Lett.* **88**, 173116 (2006).

⁵Y. H. Zhao, J. F. Bingert, X. Z. Liao, B. Z. Cui, K. Han, A. V. Sergueeva, A. K. Mukherjee, R. Z. Valiev, T. G. Langdon, and Y. T. Zhu, *Adv. Mater.* **18**, 2949 (2006).

⁶G. D. Chu, Y. H. Wei, D. Z. Li, and Y. Tian, *Iron Steel Res. Int.* **18**, 331 (2011).

⁷C. Hu, S. Xia, H. Li, T. Liu, B. Zhou, W. Chen, and N. Wang, *Corros. Sci.* **53**, 1880 (2011).

⁸L. Lu, X. Chen, X. Huang, and K. Lu, *Science* **323**, 607 (2009).

⁹A. M. Hodge, T. A. Furnish, C. J. Shute, Y. Liao, X. Huang, C. S. Hong, Y. T. Zhu, T. W. Barbee, Jr., and J. R. Weertman, *Scr. Mater.* **66**, 872 (2012).

¹⁰S. Scheriau, Z. Zhang, S. Kleber, and R. Pippan, *Mater. Sci. Eng., A* **528**, 2776 (2011).

¹¹L. E. Murr, E. Moin, F. Greulich, and K. P. Staudhammer, *Scr. Metall.* **12**, 1031 (1978).

¹²G. H. Xiao, N. R. Tao, and K. Lu, *Scr. Mater.* **59**, 975 (2008).

¹³Z. S. You, L. Lu, and K. Lu, *Acta Mater.* **59**, 6927 (2011).

¹⁴J. W. Christian and S. Mahajan, *Prog. Mater. Sci.* **39**, 1 (1995).

¹⁵M. A. Meyers, O. Vöhringer, and V. A. Lubarda, *Acta Mater.* **49**, 4025 (2001).

¹⁶J. A. Venables, *Philos. Mag.* **6**, 379 (1961).

¹⁷Y. T. Zhu, X. Z. Liao, and X. L. Wu, *Prog. Mater. Sci.* **57**, 1 (2012).

¹⁸Z. W. Wang, Y. B. Wang, X. Z. Liao, Y. H. Zhao, E. J. Lavernia, Y. T. Zhu, Z. Horita, and T. G. Langdon, *Scr. Mater.* **60**, 52 (2009).

¹⁹Y. Zhang, N. R. Tao, and K. Lu, *Scr. Mater.* **60**, 211 (2009).

²⁰X. Z. Liao, F. Zhou, E. J. Lavernia, D. W. He, and Y. T. Zhu, *Appl. Phys. Lett.* **83**, 5062 (2003).

²¹X. Z. Liao, F. Zhou, E. J. Lavernia, S. G. Srinivasan, M. I. Baskes, D. W. He, and Y. T. Zhu, *Appl. Phys. Lett.* **83**, 632 (2003).

²²M. Chen, E. Ma, K. J. Hemker, H. Sheng, Y. Wang, and X. Cheng, *Science* **300**, 1275 (2003).

²³S. Ni, Y. B. Wang, X. Z. Liao, H. Q. Li, R. B. Figueiredo, S. P. Ringer, T. G. Langdon, and Y. T. Zhu, *Phys. Rev. B* **84**, 235401 (2011).

²⁴H. Fujita and T. Mori, *Scr. Metall.* **9**, 631 (1975).

²⁵C. S. Hong, N. R. Tao, K. Lu, and X. Huang, *Scr. Mater.* **61**, 289 (2009).

²⁶G. T. Gray, *Acta Metall.* **36**, 1745 (1988).

²⁷Y. Cao, Y. B. Wang, S. N. Alhajeri, X. Z. Liao, W. L. Zheng, S. P. Ringer, T. G. Langdon, and Y. T. Zhu, *J. Mater. Sci.* **45**, 765 (2010).

²⁸Y. Cao, Y. B. Wang, R. B. Figueiredo, L. Chang, X. Z. Liao, M. Kawasaki, W. L. Zheng, S. P. Ringer, T. G. Langdon, and Y. T. Zhu, *Acta Mater.* **59**, 3903 (2011).

²⁹A. P. Zhilyaev and T. G. Langdon, *Prog. Mater. Sci.* **53**, 893 (2008).

³⁰R. B. Figueiredo, P. R. Cetlin, and T. G. Langdon, *Mater. Sci. Eng. A* **528**, 8198 (2011).

³¹X. Zhang, A. Misra, H. Wang, T. D. Shen, M. Nastasi, T. E. Mitchell, J. P. Hirth, R. G. Hoagland, and J. D. Embury, *Acta Mater.* **52**, 995 (2004).

³²G. Saada and J. Douin, *Philos. Mag. Lett.* **64**, 67 (1991).

³³V. Yamakov, D. Wolf, S. R. Phillpot, and H. Gleiter, *Acta Mater.* **50**, 5005 (2002).

³⁴Y. B. Wang and M. L. Sui, *Appl. Phys. Lett.* **94**, 021909 (2009).

³⁵S. Ni, Y. B. Wang, X. Z. Liao, R. B. Figueiredo, H. Q. Li, S. P. Ringer, T. G. Langdon, and Y. T. Zhu, *Acta Mater.* **60**, 3181 (2012).

³⁶X. Z. Liao, J. Y. Huang, Y. T. Zhu, F. Zhou, and E. J. Lavernia, *Philos. Mag.* **83**, 3065 (2003).

³⁷C. X. Huang, K. Wang, S. D. Wu, Z. F. Zhang, G. Y. Li, and S. X. Li, *Acta Mater.* **54**, 655 (2006).

³⁸M. Qwamizadeh, M. Kadkhodaei, and M. Salimi, *Int. J. Adv. Manuf. Technol.* **61**, 227 (2012).

³⁹K. Renard, H. Idrissi, D. Schryvers, and P. J. Jacques, *Scr. Mater.* **66**, 966 (2012).

⁴⁰D. H. Shin, I. Kim, J. Kim, Y. S. Kim, and S. L. Semiatin, *Acta Mater.* **51**, 983 (2003).

⁴¹Y. H. Zhao, X. Z. Liao, Z. Horita, T. G. Langdon, and Y. T. Zhu, *Mater. Sci. Eng., A* **493**, 123 (2008).

⁴²Y.-Y. Chao and S. K. Varma, *Scr. Metall. Mater.* **24**, 1665 (1990).

⁴³L. L. Shaw, A. L. Ortiz, and J. C. Villegas, *Scr. Mater.* **58**, 951 (2008).

⁴⁴X. Zhang and A. Misra, *Scr. Mater.* **66**, 860 (2012).